1923 Gleno Dam Break: Case Study and Numerical Modeling

Marco Pilotti[1]; Andrea Maranzoni[2]; Massimo Tomirotti[3]; and Giulia Valerio[4]

Abstract: On the morning of December 1, 1923, the Gleno Dam (located in the Central Italian Alps) suddenly collapsed a few days after the first complete reservoir filling. Nearly 4.5×10^6 m^3 of water was released. The consequent inundation caused significant destruction along the downstream valley and a death toll of at least 356 lives. This failure is the only historical case of dam break caused by structural deficiencies that has occurred in Italy. As a result, it has deeply influenced the evolution of Italian regulations regarding dam design and hydraulic risk evaluation. However, in spite of its relevance, this event has never been characterized from a hydraulic standpoint. This paper reports the main information obtained from the analysis of a vast amount of historical documents regarding the Gleno Dam break to set up a case study useful for validating dam-break models in mountain settings. Moreover, it presents the main results of one-dimensional (1D) modeling of the dam break wave propagation accomplished with a first-order finite volume numerical scheme recently proposed in the literature for field applications. The overall effectiveness and reliability of the model are evaluated for this case characterized by very irregular topography. Finally, the practical relevance of several choices that the numerical reconstruction of this kind of event demands is tested. **DOI: 10.1061/(ASCE)HY.1943-7900.0000327.**

CE Database subject headings: Dam failures; Shallow water; Numerical models; Hydraulic models; Case studies; Italy.

Author keywords: Dam failure; 1D dam-break modeling; Shallow water; Finite volume numerical model; Hydraulic hazard; Case study.

Introduction

Despite technological advances in recent decades, the worldwide safety of dams does not appear to have greatly improved since the major failure rate in the period between 1946 and 1955 almost doubled in the following decade (Johnson and Illes 1976; Singh 1996), with a rising trend toward the end of the last century (Donnelly and Morgenroth 2005; Saxena and Sharma 2004). At the same time, several survey and monitoring studies (e.g., Douglas et al. 1998) have reckoned that the annual probability of a major dam failure is in the order of 10^{-4}, which is one order of magnitude lower than the probability usually assumed for the design of spillways. Accordingly, in spite of its very small probability of occurrence, dam failures are, to a certain extent, unavoidable, as a consequence of structural deficiencies (approximately 60% of the recorded accidents), inadequate spilling design or inaccurate design flood estimation (30%), and, finally, landslides that can cause dam overtopping in the reservoir (10%) (Singh 1996). In the future, climate change and progressive structural deterioration of the oldest dams might play a significant role in modifying these percentages, while the continuous and rapid growth of built-up zones in the tailwater areas will significantly increase the exposure level.

Given this state of affairs, the problem of dam safety assessment is of considerable importance, and in many countries national technical legislation requires delineation of areas that would be flooded in the event of dam failure. Accordingly, predicting the flood propagation effects following a hypothetical dam failure is an indispensable requirement both for land-planning purposes and for the formulation of disaster contingency plans.

In this direction, the approach widely accepted is based on the shallow water equations (SWE), since they best combine computational efficiency and accurate reconstruction of the physical phenomenon, as clearly shown by recent scientific literature (e.g., Soares Frazão et al. 2000, 2003) produced by the important European projects Concerted Action on Dambreak Modelling (CADAM) and Investigation of Extreme Flood Processes and Uncertainty (IMPACT). In particular, general agreement exists that SWE can be used to describe dam-break waves even when they take place over real topography (Hervouet and Petitjean 1999; Valiani et al. 2002; Begnudelli and Sanders 2007; Aureli et al. 2008b; Natale et al. 2008; Pilotti et al. 2010). However, in the presence of very irregular topography characterized by steep bed slopes as in mountain regions, the key SWE assumptions of small bed slopes and negligible vertical acceleration (e.g. Cunge et al. 1980; Toro 2001) are violated. Therefore, in this context it seems important to evaluate their applicability (Pilotti et al. 2006, 2010).

The ultimate confidence in the use of a mathematical model is based on the comparison of its performance with known test cases. Usually these test cases are analytical solutions that can be derived under restrictive geometrical conditions that are not satisfied in field applications. For this reason, it is desirable to have field test cases to verify the accuracy, robustness, and effectiveness of both the adopted mathematical model and numerical scheme. Although field tests do not allow comparisons as precise as analytical

[1]Associate Professor, DICATA, Univ. of Brescia, Via Branze 43, 25123 Brescia, Italy (corresponding author). E-mail: marco.pilotti@ing.unibs.it

[2]Researcher, DICATA, Univ. of Brescia, Via Branze 43, 25123 Brescia, Italy. E-mail: andrea.maranzoni@unipr.it

[3]Associate Professor, DICATA, Univ. of Brescia, Via Branze 43, 25123 Brescia, Italy. E-mail: massimo.tomirottiing@ing.unibs.it

[4]Ph.D. Student, DICATA, Univ. of Brescia, Via Branze 43, 25123 Brescia, Italy. E-mail: giulia.valerio@ing.unibs.it

Note. This manuscript was submitted on July 2, 2009; approved on September 3, 2010; published online on September 7, 2010. Discussion period open until September 1, 2011; separate discussions must be submitted for individual papers. This paper is part of the ***Journal of Hydraulic Engineering***, Vol. 137, No. 4, April 1, 2011. ©ASCE, ISSN 0733-9429/2011/4-480–492/$25.00.

solutions, in our opinion they provide an overall direct evaluation of the actual engineering effectiveness of the tested model. Unfortunately, according to Garcia (2007), "there is very little information to test, calibrate and validate mathematical models that could potentially be used to mitigate the impact of catastrophic flows." Actually, in the literature only a handful of historical dam-break test cases is sufficiently documented, including the events of Malpasset (James 1988; CADAM 1999; Goutal 1999), Tous (Alcrudo and Mulet 2007), St. Francis (Begnudelli and Sanders 2007), and Sella Zerbino (Natale et al. 2008). To our knowledge, in none of these cases did the dam-break wave propagate in very steep valley bathymetry. Only in a few other field cases, in which the flood wave caused geomorphic effects that in turn significantly affected the flow, do complete data sets well suited for testing morphological models exist (Jarrett and Costa 1986; Capart et al. 2007). Also experimental data derived from field physical models are very rare (e.g., De Marchi 1945; Hervouet and Petitjean 1999). On the contrary, more frequently, one finds in the literature laboratory data concerning dam-break flows in idealized configurations, both with movable bed (e.g., Capart and Young 1998; Spinewine and Zech 2007) and fixed bed (e.g., Soares Frazão and Zech 2007; Aureli et al. 2008a).

To provide further data useful for model testing, we present in this paper the historical case of the Gleno Dam break, which happened on December 1, 1923, in the Italian Alps. This accident is the only important historical case of dam break produced by structural deficiencies that occurred in Italy. About 4.5×10^6 m^3 of water retained in the reservoir were released in a few minutes when a central part of the dam measuring approximately 80 m collapsed, causing at least 356 casualties and huge destruction along the 21 km downstream valley. The aftermath of this catastrophe was so intense as to gain mention even in the international technical literature (De Martini 1924; Stucky 1924) and it deeply influenced the evolution of Italian regulations and their administration regarding dam design and hydraulic hazard evaluation (Maugliani 2004). In spite of its relevance, this accident, already well documented from a historical and structural point of view (Ganassini and Danusso 1924; De Martini 1924; Stucky 1924; Pedersoli 1973), has never been characterized from a hydraulic standpoint.

In this paper, we reconstruct this event by recovering a great deal of information that can be used for modeling purposes. Because no topographic survey from before 1923 was available for the area of interest, we have carefully reproduced the valley bathymetry presumably existing before the accident by means of a 5×5 m digital elevation model (DEM) corrected based on available historical documents. The dynamics of the reservoir emptying is described through a two-dimensional (2D) shallow water simulation; the outflow discharge hydrograph computed at the dam location provides the upstream boundary condition for the one-dimensional (1D) simulation of the dam-break wave propagation along the downstream valley. The narrowness of this valley with respect to the huge discharges involved justifies the adoption of the 1D schematization. We have employed the finite-volume first-order numerical scheme presented by Capart et al. (2003), specifically proposed for flood modeling over natural bathymetries. This method is based on an approximate formulation of the momentum conservation equation where the geometric source terms due to bed steepness and lack of prismaticity are included in the flux term, thus allowing a strict fulfillment of the *C*-property. The flux term is computed according to the Pavia flux predictor (PFP) upwind technique proposed by Braschi and Gallati (1992).

To obtain quantitative information on the flooding extent and dynamics to be compared with the numerical results, a rich historical documentation compiled from several archives has been retrieved. The documentation includes old photographic images, reliable testimonies, and various written documents.

A sensitivity analysis of grid size, roughness, and the inflow hydrograph was conducted to clarify the practical scope of these aspects. All the information collected and the data useful for the numerical simulation are made available to the user community at the ASCE Library (http://www.ascelibrary.org) and on the website http://www.ing.unibs.it/~idraulica/gleno_testcase.htm.

The Gleno Dam Break

The Gleno Dam (46°01′00″ N, 10°04′30″ E) is located in Valle del Povo, a small subcatchment of approximately 8.4 km^2 in Valle di Scalve (174 km^2), a main tributary valley of Valle Camonica (1460 km^2) in Lombardy (see Fig. 1 and File S9). The annual mean discharge at the dam section can be estimated at 0.37 m^3/s.

In the original design submitted in 1913, this dam was a masonry gravity dam with a curvilinear planimetric layout to create a reservoir with a maximum capacity of about 5×10^6 m^3. Construction started in 1917. Soon after a stone masonry basement to close the lower part of the valley was constructed, the original design was replaced by a slender reinforced concrete structure of the multiple-arch type, with the central curved section resting over the masonry basement. The dam had an S-shaped planimetry, comprising a circular central portion about 70 m long and straight end portions, for an overall length of 220 m. It was 46 m high and consisted of 25 arches in all, resting on concrete spurs founded partly on the masonry base, partly on the rock of the valley side (Fig. 2).

In the early morning of December 1, 1923, about 40 days after the first complete reservoir filling, an 80 m long breach opened in the central portion of the Gleno Dam (Fig. 3). As the subsequent technical examinations proved (Ganassini and Danusso 1924), the collapse was triggered by water seepage at the interface between the masonry base and the overlying structure. The effects of the flood propagation along the downstream river were catastrophic. The flood wave took about 45 min to flush the nearly 21 km-long valley downstream of the dam as far as Darfo (Fig. 1). Along with the death toll, the flood destroyed three villages, five power stations, and finally a high number of isolated buildings and factories.

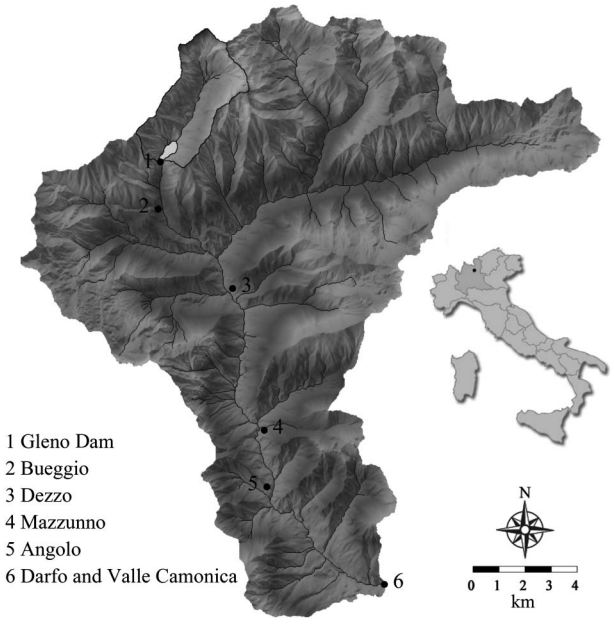

Fig. 1. Location of the Gleno Dam in Valle di Scalve

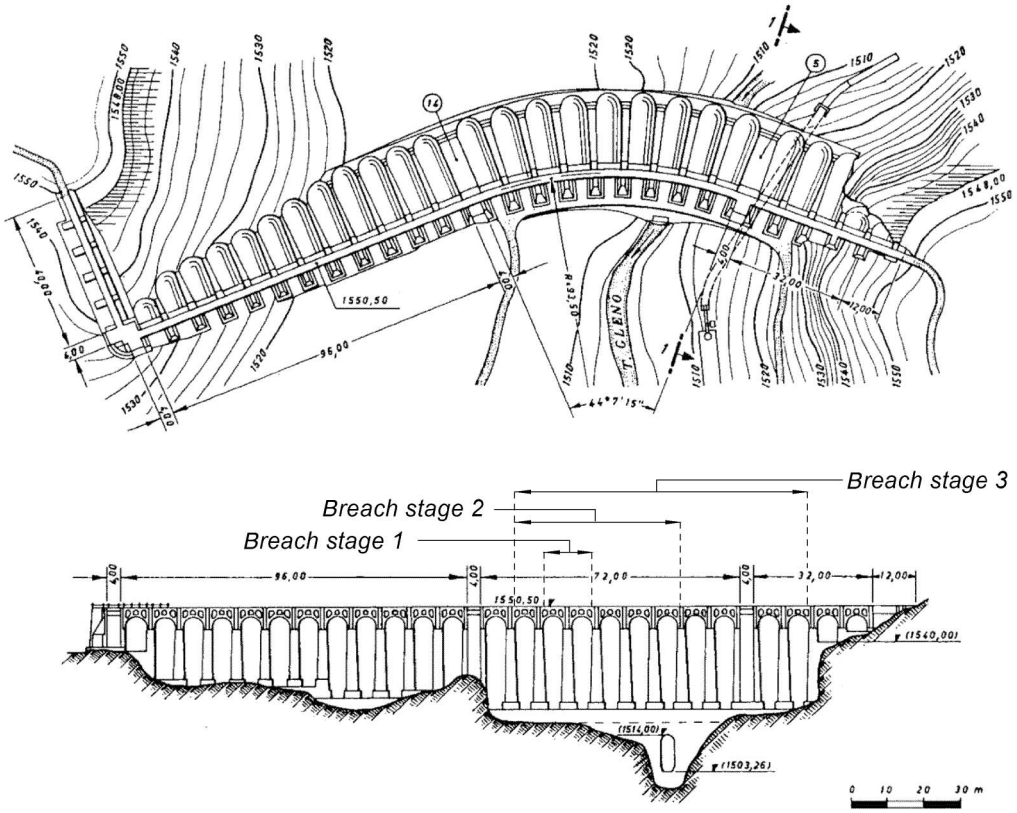

Fig. 2. Plan and elevation views of the Gleno Dam (modified from ANIDEL 1961, with permission)

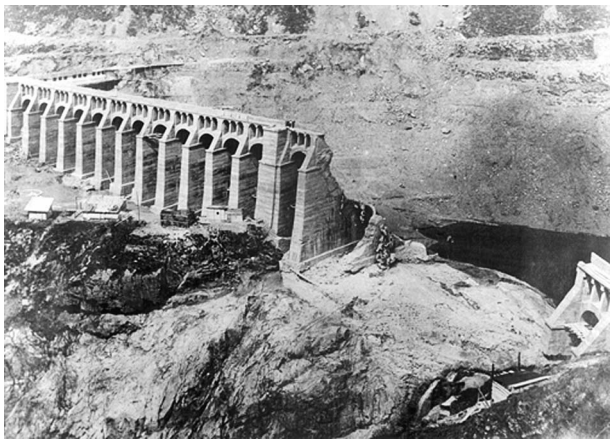

Fig. 3. The remains of the Gleno Dam with the breach (photo courtesy of Foto Giorgio)

The Gleno disaster shocked the Italian public so much that many reports were published in the newspapers and hundreds of pictures were taken, some of which are shown in File S10. As a consequence of this catastrophic event, the multiple-arch design, in itself not responsible for the accident, was almost completely abandoned in Italy.

Data Available for Gleno Dam-Break Modeling

The Gleno accident can be sufficiently documented to prepare a test case to evaluate the effectiveness of the numerical algorithms for dam-break modeling in mountain regions. Actually, the previous field dam-break test cases presented in the literature (Goutal 1999; Alcrudo and Mulet 2007; Begnudelli and Sanders 2007), with the only exception of the Lawn Lake case (Jarrett and Costa 1986), are related to fairly flat topographies when compared with the Gleno one, in which the flood propagated through a narrow and steep mountain valley, with a thalweg drop of nearly 1,250 m along a total length of nearly 21 km. The bed slope is on average about 6%, but locally it is higher than 90% in the upper reach [Fig. 4(a)].

The gathered historical information (mainly retrieved from the 16 major documentary sources listed in File S15) includes photographic images of the inundation effects (enclosed in the downloadable File S10), survivors' testimonies, and technical relations concerning the causes of the event (gathered in File S4), and finally, designs of the constructions built in the aftermath with hydraulic restoration purposes.

Bed Bathymetry

The most destructive effects of the flood propagation occurred along the Valle di Scalve, from the Gleno Dam down to the village of Darfo, at the confluence in the Oglio River (Fig. 1). Unfortunately, no sufficiently detailed topographical maps antecedent to the event exist for the whole area. Therefore, to reconstruct the bathymetry, we have digitized 20 year-old paper maps at scale 1:10,000 with contour lines every 10 m, in addition to many scattered single elevation points and points along the thalweg line.

Since the valley is mostly carved in rock, both in the upper part where very compact metamorphic rocks and red sandstone are found and in the lower part where compact calcareous layers prevail, the effects of the flood erosive action were localized. Some historical photos clearly show that morphological changes occurred in some zones mainly located in the upper part of the valley (see File S10). Based on the documents available, we have identified these areas and also the locations where some hydraulic structures were built during the following decades. Accordingly, the valley

bathymetry has been carefully and locally modified to reproduce a topography as close as possible to the one originally existing before the accident. Only in correspondence of the small village of Bueggio (Fig. 1) it has not been possible to ascertain the original width of the valley. The resulting Cartesian DEM covering the region of interest has a 5×5 m resolution and consists of more than 6.66×10^6 elevation points; it is available within File S3. The contour map of the reconstructed bathymetry is reported in Fig. 4(b).

During the flood, some bridges were swept away. In addition, some villages, several power houses, and buildings located along the river were destroyed. We have decided not to document the position of these obstacles because we believe that the destructive interaction of the flood with these details had limited implications on the overall propagation.

For the 1D modeling of the flood propagation, we provide in downloadable File S12 a list including the location of more than 1,300 valley cross-sections that have been extracted orthogonally to the channel. The hydraulic and geometrical characteristics of each cross-section are reported in tabular form in File S14.

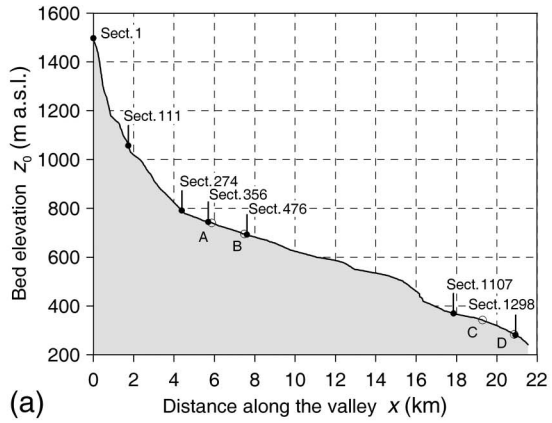

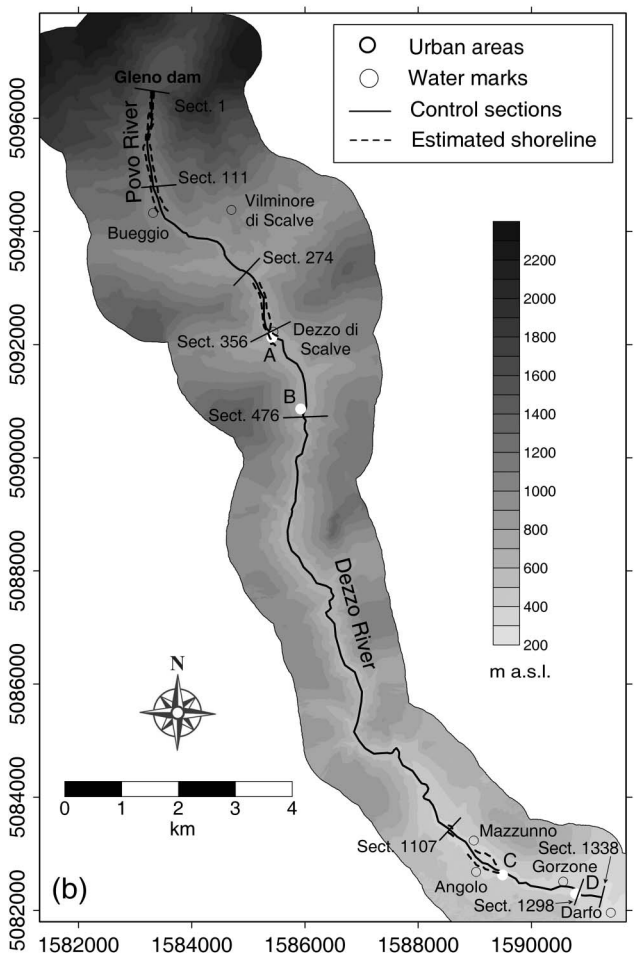

Fig. 4. (a) Longitudinal profile of the thalweg and (b) contour map of the reconstructed bathymetry of the valley [Italian Gauss-Boaga reference system (m)]

Roughness Coefficient

The only parameter appearing in the shallow water model is the Manning's coefficient. To document the valley roughness, a comprehensive set of nine pictures along with their position in the valley is provided in File S13. Based on these pictures and the information on the planimetric and altimetric pattern of the thalweg, we have hypothesized a Manning's coefficient ranging between 0.05 $s/m^{1/3}$ and 0.10 $s/m^{1/3}$, as documented in the literature for strongly irregular and densely vegetated mountain valleys (e.g., Barnes 1967; Jarrett 1984).

Boundary Conditions

To simulate the flood propagation, the hydrograph of the discharge flowing out of the breach must be estimated and imposed at the upstream boundary of the computational domain. Moreover, the water level hydrograph at the dam site provides the additional upstream boundary condition required by an upwind type numerical scheme when the flow entering the computational domain is supercritical.

The peculiarity of the Gleno Dam break in comparison with the other documented historical cases is the presence of an eyewitness: the dam watchman who was literally under the dam when the failure happened. From his trial testimony (see File S4), four important facts emerged:

1. The initial water depth in the reservoir was approximately 38 m, slightly higher than the maximum allowed.
2. The failure happened at 7:05 a.m; this piece of information must be compared with the information regarding the arrival of the wave surge at the village of Darfo (7:50–7:55 a.m.).
3. The collapse of the dam buttresses was very rapid and happened in three stages. The eleventh spur fell first, along with the two arches resting on it, causing a breach whose width can be estimated to be about 14 m. Shortly after, Spurs 8 to 12 fell, widening the breach to 48 m. Eventually, Spurs 4 to 7 also fell, causing an overall final breach width of 80 m (see Solid Lines 1, 2, and 3 overlying Fig. 2).
4. The emptying time of the reservoir was estimated to be 12–15 min.

Since the breach evolution is reasonably well identified, we have evaluated the outflow hydrograph by simulating the reservoir emptying. In view of the essentially 2D feature of this process, we have numerically solved the 2D SWE (some results are shown in File S7). To this purpose, we have employed a numerical code based on the well-known MacCormack finite difference scheme. This model has been carefully validated based on the usual test cases proposed in the literature (Pilotti et al. 2010). Moreover, a 4 m DEM of the bathymetry of the Gleno reservoir has been reconstructed (Fig. 5) according to the same procedure described for the tailwater valley (see File S6). Although the effect of vertical acceleration is neglected in this 2D schematization, as far as the discharge hydrograph in partial dam break is concerned, the differences related to a better description of the 3D flow field around the breach are, from an engineering point of view, totally negligible (Pilotti et al. 2010).

To compute the hydrograph following the failure, it was necessary to specify the time lag between the three phases of the collapse.

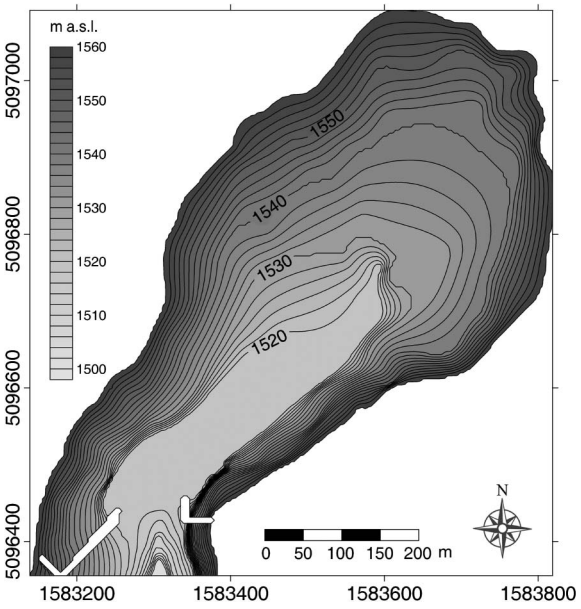

Fig. 5. Bathymetry of the Gleno Reservoir [Italian Gauss-Boaga reference system (m)]

Although, based on the testimony of the witness, the time lag between the first and the second stage in the breach development cannot be much longer than 30 s, a direct indication of the time lag to the final stage of the process does not exist. However, since it seems reasonable that the final collapse took place very rapidly, we have supposed that the final stage took 30 s. In addition to the described collapse scenario (Scenario B), we have also considered a sudden removal of the whole breach (Scenario A).

Fig. 6 shows the two discharge and water depth hydrographs that have been computed by the solution of 2D SWE. In both cases

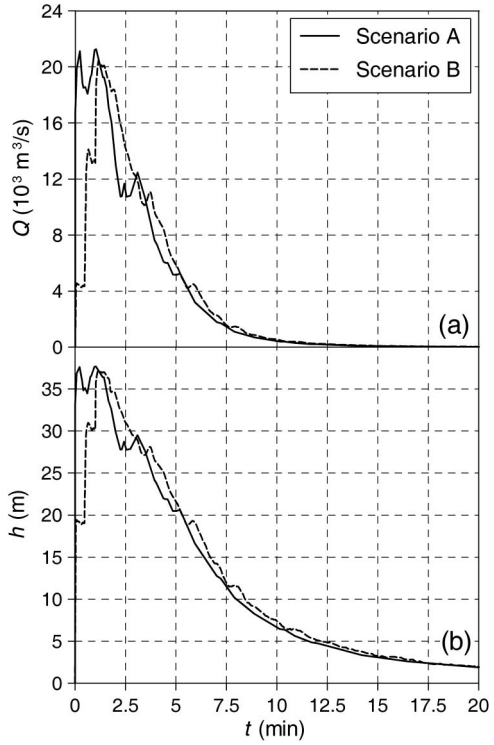

Fig. 6. (a) Discharge and (b) water level time series at the breach section for the cases of sudden failure (Scenario A) and collapse duration of 1 min (Scenario B)

the emptying time is in very good agreement with the observed 12–15 min reported by the witness.

At the downstream end of the investigated river stretch, a free outflow (transmissive) boundary condition has been applied.

Initial Condition

Comparing the dam break peak discharge (in the order of 10^4 m^3/s at the dam location) with the natural discharges typical of the river downstream (e.g., the 1,000 year return period discharge at Darfo might be evaluated at 500 m^3/s by using a regional model), a dry bed initial condition seems a reasonable assumption in the numerical simulation.

Envelope of Flooded Areas

The inspected documentary material was sufficient to characterize the inundation dynamics. Unfortunately, no report delineating the extent of the inundation has been found. However, many pictures taken in the days following the disaster (see File S10) can be used to evaluate the flood extent.

This type of reconstruction can be performed by means of photogrammetric software that requires careful information regarding the orientation parameters of the camera or, alternatively, at least four fixed points of known locations. Since these data are not available for the old photographic plates, we have devised an imaging procedure based on the superimposition between the historical image and a corresponding 3D virtual image created from the DEM of the valley (see Fig. 7). This virtual image can be created by using some commercial software packages that reproduce the valley bathymetry as seen from a specified point of view with the same perspective as the original picture [Fig. 7(b)], and superimposing it on the reference historical image [Fig. 7(c)]. Some other examples are provided in File S16. To achieve a more reliable result, it is better to locate some georeferenced landmarks within the DEM (e.g., the penstock along the left mountainside in Fig. 7(a), a road, or some existing buildings) that are evident in the original picture. By working on the compound image, the outline of the flooded area can finally be digitized and georeferenced, as shown subsequently in Fig. 10. We have obtained the envelope of the flooded area for a stretch totalling about 5 km out of the overall 21 km length of the valley [Fig. 4(b)]. These data are included in File S5.

In addition to the distributed information regarding the flood extent, the comparative analysis of documents and isolated pictures allows a more precise estimation of the maximum water level reached during the inundation at some locations. These water marks are shown in Fig. 4(b) and listed in File S17.

Numerical Modeling of the Gleno Dam Break

Despite the restrictive shallow water hypotheses, the de Saint-Venant equations are widely accepted in the literature today as an effective tool to model flood propagation in streams, even in the presence of a steep bottom slope. Moreover, it has been shown that strong free surface curvature only locally affects the process (e.g., Mohapatra and Chaudry 2004). Nevertheless, particularly in field applications, the computation of the geometric source term is certainly a major stumbling block. The approach recently proposed by Capart et al. (2003) provides an innovative way to cope with this problem, although some additional difficulties arise when steep bathymetries must be handled.

We have adopted a 1D schematization, suggested by the valley geometry with respect to the involved discharges. Since the valley flushed by the flood is largely cut in the bedrock, the fixed bed assumption seemed reasonable. Although the Gleno disaster was

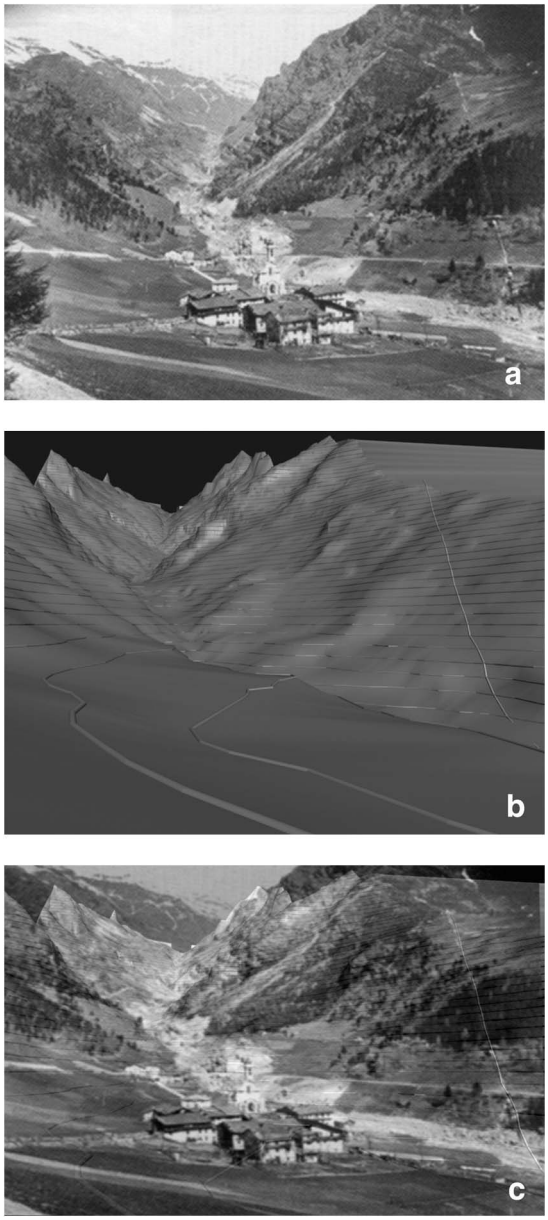

Fig. 7. Example of flood envelope estimation from photographic documents: (a) historical image of the village of Bueggio after the wave passage; (b) corresponding 3D virtual image reconstructed from the DEM; (c) superimposition of historical and virtual images (photo courtesy of Foto Giorgio)

certainly characterized by massive sediment and floatable transport, the overall phenomenology was not that of a debris flow because of the strong dilution by the huge volume of water. Finally, biphasic unsteady modeling in field applications is still beset by very high levels of uncertainties. By pursuing the fixed-bed hypothesis, we have also a hint of the relevance, at the basinwide scale, of the consequences of this simplifying assumption.

Governing Equations

The 1D de Saint-Venant equations in integral form read (e.g., Cunge et al. 1980)

$$\frac{d}{dt}\int_{x_1}^{x_2}\mathbf{U}(x,t)dx+\mathbf{F}(\mathbf{U}(x_2,t))-\mathbf{F}(\mathbf{U}(x_1,t))=\int_{x_1}^{x_2}\mathbf{S}(\mathbf{U}(x,t))dx \tag{1}$$

where

$$\mathbf{U}=\begin{pmatrix}A\\Q\end{pmatrix},\qquad \mathbf{F}=\begin{pmatrix}Q\\Q^2/A+gI_1\end{pmatrix},\qquad \mathbf{S}=\begin{pmatrix}0\\gA(S_0-S_f)+gI_2\end{pmatrix} \tag{2}$$

The conserved variables A and Q represent, respectively, the wetted cross-sectional area and the discharge, x indicates the distance along the thalweg, and t, the time variable; g is the acceleration due to gravity. The terms I_1 and I_2 denote the first moment of the wetted area with respect to the free surface and the term of nonprismaticity

$$I_1=\int_0^{h(x)}(h-\eta)b(x,\eta)d\eta,\qquad I_2=\int_0^{h(x)}(h-\eta)\frac{\partial b}{\partial x}d\eta \tag{3}$$

where h = water depth and $b(x,\eta)$ = cross-sectional width at height η on the local thalweg. Finally, in Statement (2) S_0 is the bed slope and S_f, the friction slope, usually computed by the Manning formula

$$S_f=\frac{n_f^2|Q|Q}{A^2R^{4/3}} \tag{4}$$

in which n_f is the Manning's roughness coefficient and R the hydraulic radius.

The adoption of the classical formulation [Eqs. (1) and (2)] of the SWE presents some problems in field applications. The bathymetry of natural valleys is often very irregular, and the topographical description of the reach of interest is usually given by means of a limited number of cross sections. Therefore, an accurate estimate of the terms S_0 and I_2 is arduous (Garcia-Navarro et al. 1999; Capart et al. 2003). To overcome these difficulties, Capart et al. (2003) proposed an approximate evaluation of the pressure force acting on wetted lateral and bottom boundary surface. It follows a modified form of Eq. (1) in which the geometric source term is written in divergence form: bottom slope and nonprismaticity effects are no longer considered geometric forcing terms, as usual, but are transferred within the momentum flux. Consequently, Statement (2) is changed as

$$\mathbf{U}=\begin{pmatrix}A\\Q\end{pmatrix},\qquad \mathbf{F}=\begin{pmatrix}Q\\Q^2/A+gI_1-gI_1|_{\bar{z}}\end{pmatrix},\qquad \mathbf{S}=\begin{pmatrix}0\\-gAS_f\end{pmatrix} \tag{5}$$

in which $I_1|_{\bar{z}}$ is the first moment with respect to the water surface calculated assuming the averaged water surface elevation $\bar{z}$ over the interval $[x_i, x_{i+1}]$. As shown by Capart et al. (2003) and then by Chen et al. (2007), Eq. (1) combined with Eq. (5) could replace the system [Eqs. (1) and (2)] without introducing remarkable inaccuracies within the framework of the SWE, and in general for most practical situations, even in the presence of hydraulic jumps or shock waves.

Numerical Scheme

In mountain areas the topography is usually very irregular and is characterized by abrupt changes in bottom slope and cross-section geometry that can induce transcritical flow regimes and the formation of shock waves in flood propagation. All these aspects require ad hoc numerical methods that effectively solve the SWEs combining the shock-capturing property with robustness, versatility, and stability characteristics.

Over the last years, the finite volume method has earned a great success (Toro 2001; LeVeque 2002) and is currently used in these kinds of applications (Valiani et al. 2002; Alcrudo and Mulet 2007; Begnudelli and Sanders 2007; Aureli et al. 2008b). In the finite volume framework, the explicit updating algorithm for the discretized variable $\mathbf{U}_i$ over the i-cell Δx_i is

$$\mathbf{U}_i^{n+1} = \mathbf{U}_i^n - \frac{\Delta t^n}{\Delta x_i}(\mathbf{f}_{i+1/2} - \mathbf{f}_{i-1/2}) + \Delta t^n \mathbf{S}_i \tag{6}$$

where the superscript n denotes the n-time step, while $\mathbf{f}_{i\pm1/2}$ are the intercell numerical fluxes; $\mathbf{S}_i$ is the approximation of the source term. The first-order algorithm proposed by Capart et al. (2003) is based on the approximated formulation [Eqs. (1)–(5)] of the de Saint-Venant equations and makes use of the PFP upwind scheme suggested by Braschi and Gallati (1992) for the numerical flux prediction. Introducing the Froude number F and the celerity c, the numerical estimation of the flux vector components Q^* and Σ^* is obtained by linear discretization of characteristic and compatibility equations

$$\text{for } \mathsf{F}_{i+1/2}^n > 1 \begin{cases} Q_{i+1/2}^* = Q_i^n - \frac{c_i^n + c_{i+1}^n}{4}(A_i^n|_{\bar{z}} - A_{i+1}^n|_{\bar{z}}) \\ \Sigma_{i+1/2}^{*\text{left}} = \frac{(Q_i^n)^2}{A_i^n} \\ \Sigma_{i+1/2}^{*\text{right}} = \frac{(Q_i^n)^2}{A_i^n} + g(I_1)_i^n - g(I_1)_i^n|_{z_{i+1}} \end{cases} \tag{7}$$

$$\text{for } \mathsf{F}_{i+1/2}^n \le 1 \begin{cases} Q_{i+1/2}^* = \frac{1+\mathsf{F}_{i+1/2}^n}{2} Q_i^n + \frac{1-\mathsf{F}_{i+1/2}^n}{2} Q_{i+1}^n + \frac{c_i + c_{i+1}}{4}[1 - (\mathsf{F}_{i+1/2}^n)^2](A_i^n - A_{i+1}^n) - \frac{c_i^n + c_{i+1}^n}{4}(A_i^n|_{\bar{z}} - A_{i+1}^n|_{\bar{z}}) \\ \Sigma_{i+1/2}^{*\text{left}} = \frac{1+\mathsf{F}_{i+1/2}^n}{2}\frac{(Q_i^n)^2}{A_i^n} + \frac{1-\mathsf{F}_{i+1/2}^n}{2}\left[\frac{(Q_{i+1}^n)^2}{A_{i+1}^n} + g(I_1)_{i+1}^n - g(I_1)_{i+1}^n|_{z_i}\right] + \frac{c_i^n + c_{i+1}^n}{4}[1 - (\mathsf{F}_{i+1/2}^n)^2](Q_i^n - Q_{i+1}^n) \\ \Sigma_{i+1/2}^{*\text{right}} = \frac{1+\mathsf{F}_{i+1/2}^n}{2}\left[\frac{(Q_i^n)^2}{A_i^n} + g(I_1)_i^n - g(I_1)_i^n|_{z_{i+1}}\right] + \frac{1-\mathsf{F}_{i+1/2}^n}{2}\frac{(Q_{i+1}^n)^2}{A_{i+1}^n} + \frac{c_i^n + c_{i+1}^n}{4}[1 - (\mathsf{F}_{i+1/2}^n)^2](Q_i^n - Q_{i+1}^n) \end{cases} \tag{8}$$

where $\mathsf{F}_{i+1/2}^n = (V_i^n + V_{i+1}^n)/(c_i^n + c_{i+1}^n)$, V = velocity, and $\bar{z} = \alpha z_i + (1-\alpha)z_{i+1}$, α being a weighting coefficient ($0 \le \alpha \le 1$). Although Chen et al. (2007) have suggested that for natural streams a value of α between 0.5 and 1.0 may be appropriate, especially where sudden valley expansions and contractions take place, here, following Capart et al. (2003), we adopt $\alpha = 0.5$.

In Eqs. (7) and (8), the geometrical correction term $(I_1)_i^n|_{z_{i+1}}$ represents the first moment with respect to the water surface computed in the i-section for piezometric head z_{i+1} calculated in the $i+1$-section at the time level n; the Σ^* term is evaluated differently on the two sides of the same boundary cell; this "lateralization" of the momentum flux—as defined in Capart et al. (2003)—reflects the nonconservative effect of the geometric forcing terms.

Concerning the friction source term evaluation, the pointwise semi-implicit treatment (Garcia-Navarro et al. 1999)

$$S_{f_i} = \frac{n_{fi}^2 |Q_i^n| Q_i^{n+1}}{(A_i^n)^2 (R_i^n)^{4/3}} \tag{9}$$

has been preferred to prevent unphysical flow inversions. In addition, the boundary conditions have been implemented as in Capart et al. (1999), in accordance with the upwind architecture of the scheme.

To properly track the wetting and drying fronts, and avoiding the well-known stability problems (Toro 2001), the algorithm is applied only to computational cells in which $h_i \ge \varepsilon$, where ε is a suitably small positive tolerance. Finally, the usual Courant-Friedrichs-Lewy stability condition controls the computation of the time step Δt^n

$$\Delta t^n = \mathsf{Cr} \min\left\{\frac{\Delta x_i}{|Q_i^n/A_i^n + \sqrt{gA_i^n/b_i^n}|}\right\} \tag{10}$$

In the following simulations ε has been set at 10^{-4} m and the Courant number Cr at 0.9.

Properties and Difficulties

As Capart et al. (2003), Pilotti et al. (2006), and Chen et al. (2007) verified with the reference test cases usually considered in the literature and with field case studies, the adopted numerical scheme is effective and robust and assures satisfactory performance. In particular, it is shock-capturing and capable of dealing with continuous transcritical transitions, and it exactly preserves the static condition even on irregular topographies (C-property). Nevertheless, despite its suitability in unsteady river-flow modeling over natural topography, this scheme requires a very fine computational mesh in the presence of a steep water surface slope combined with steep bathymetry (Capart et al. 2004). This kind of spatial discretization can involve a considerable computational effort. Actually, when the topography presents high slopes, as in the discussed case study and the spatial discretization is not sufficiently fine with respect to the local bottom slope and water depth, water elevation in the $i+1$-section can be lower than the bottom elevation of the i-section ($z_i + 1 < z_{0i}$); this being the case, the $(I_1)_i^n|_{z_{i+1}}$ term is undefined and is set equal to zero by Capart et al. (2003) causing an underestimation of the bed slope source term.

In addition, it is desirable that the numerical scheme is capable of preserving an initial uniform flow condition. According to Eq. (6), the exact balance between friction slope and water surface slope happens if the numerical scheme strictly reproduces the equality

$$\Sigma_{i+1/2}^{*\text{left}} - \Sigma_{i-1/2}^{*\text{right}} = -gA_i S_{fi} \Delta x_i \tag{11}$$

Unfortunately this is not the case when the $(I_1)_i^n|_{z_{i+1}}$ term is evaluated according to the original expression proposed by Capart et al. (2003, 2004).

Although no general and resolutive solution was found to overcome these difficulties and preserve at the same time all the good properties of the original scheme, in this test case we propose to compute the geometric term $(I_1)_i^n|_{z_{i+1}}$ according to a first-order approximation, valid when the water surface is not discontinuous

$$(I_1)_i^n|_{z_{i+1}} = \int_0^{z_{i+1}^n - z_{0i}} (z_{i+1}^n - z_{0i} - \eta)[b(\eta)]_i^n d\eta \cong (I_1)_i^n - (S_z)_i^n \Delta x_i A_i \quad (12)$$

where $(S_z)_i^n = -(z_{i+1}^n - z_i^n)/\Delta x_i$. The main advantage of this statement is the possibility of easily computing the $(I_1)_i^n|_{z_{i+1}}$ term in all the situations, even if the bathymetry is steep and the mesh not too fine, both satisfying the C-property and maintaining an initial uniform flow condition. Unfortunately, the resulting scheme accomplishes a nonconservative discretization of the momentum equation (Cunge et al. 1980) and consequently loses the capability of correctly tracking the shock waves (Toro 2001). The introduction in Eq. (12) of the corrective second-order term $[(S_z)_i^n]^2 b_i (\Delta x_i)^2/2$, only where water elevation and water depth high gradient occur, could restore the good shock-capturing properties. However, this possibility has been rejected because it requires the definition of an effective and efficient condition for the shock identification. The plausibility of this choice within the context of the discussed case study has been verified in the "Results and Discussion" section, focusing the attention to the reach of the Scalve valley where the upstream-ward propagation of a shock wave is confirmed by the testimonies.

Sensitivity Analysis

We have accomplished a sensitivity analysis with respect to the characteristic size of the computational mesh (Hardy et al. 1999). For the sake of simplicity, we have restricted our attention to the first 4.6 km-long stretch of the stream inundated by the flood, whose morphology is representative of the whole valley.

Although the reliability of the results derived from the mathematical modeling strongly depends on the mesh quality (Samuels 1990), shared and ultimate criterions for the spacing choice are lacking in the literature. Using a specifically devised algorithm (Pilotti et al. 2006), we have extracted from the valley DEM seven different river cross-section sets, ranging from 10 to 775 sections. Table 1 provides some characteristics of these meshes. In particular, the finest mesh (Mesh 7), selected based on the refinement criterion presented in Pilotti et al. (2006), is characterized by a very small average spacing that is unusual in this kind of application; since no significant improvement to numerical results was observed in consequence of further refinement, this mesh was assumed as a reference.

Table 2 summarizes the results concerning the grid size sensitivity analysis, where the values of the L_1 error norm of the space envelope of maximum water depths and discharges are shown for different values of roughness coefficient n_f. These errors are defined as

$$E_1(h_{\max}) = \frac{1}{\sum_{i=1}^N \Delta x_i} \left(\sum_{i=1}^N \Delta x_i \frac{|h_{\max,i} - h_{\max,i}^{\text{ref}}|}{h_{\max,i}^{\text{ref}}} \right), \quad E_1(Q_{\max}^*) = \frac{1}{N} \left(\sum_{i=1}^N \frac{|Q_{\max,i+1/2}^* - Q_{\max,i+1/2}^{*\text{ref}}|}{Q_{\max,i+1/2}^{*\text{ref}}} \right) \quad (13)$$

where N is the total number of cells in each mesh, $h_{\max,i}$ and $Q_{\max,i+1/2}^*$ mean respectively the maximum values of water depth calculated in the i-cell and of discharge estimated in the $i+1/2$-boundary. Moreover, h^{ref} and Q^{ref} are reference values computed as linear interpolation of the numerical results obtained using the finest mesh. Since averaging over a cell tends to smooth the discharge profiles and underrate the peak discharge values, we have decided to consider the Q^* variable defined at the intercell boundary as

$$Q_{i\pm1/2}^* = \frac{1}{\Delta t^n} \left(\int_{t^n}^{t^{n+1}} Q(x_{i\pm1/2}, t) dt \right) \quad (14)$$

instead of the averaged quantity Q_i in the grid cell. In Table 2 the L_1 error norms show a converging trend with the grid refinement, which has been expressed also as a function of a spacing parameter obtained by normalizing each average mesh spacing with the average uniform flow depth y_{0m}, computed using the first mesh, a reference discharge $Q = 15{,}000\ \text{m}^3/\text{s}$, and a Manning coefficient $n_f = 0.075\ \text{s/m}^{1/3}$ ($y_{0m} = 12.72$ m). According to these results, a minimum grid refinement can be identified with the aim of reproducing maximum values with satisfactory accuracy. Allowing a 1% discharge error, a spatial resolution of $\Delta x_m \cong 16.3$ m (Mesh 6) would prove suitable for the numerical simulation of the Gleno Dam break.

Table 1. Different Meshes Adopted in the Sensitivity Analysis Concerning Grid Resolution

Mesh number	1	2	3	4	5	6	7
Number of cross-sections	10	19	37	72	141	281	775
Average spacing Δx_m (m)	508.4	254.1	127.0	64.4	32.6	16.3	5.9
Maximum spacing (m)	529.3	275.6	139.1	95.5	53.3	33.7	26.6
Minimum spacing (m)	484.3	233.1	115.3	57.0	27.2	12.1	3.5
Standard deviation (m)	10.74	8.24	4.83	5.83	4.32	2.92	1.77

Table 2. L_1 Error Norms of the Space Envelope of Maximum h and Q for the Different Meshes Adopted and for Different Values of the Manning Coefficient

			$n_f = 0.05\ \text{s/m}^{1/3}$		$n_f = 0.075\ \text{s/m}^{1/3}$		$n_f = 0.10\ \text{s/m}^{1/3}$	
Mesh number	N	Spacing param. $\Delta x_m/y_{0m}$ (-)	E_1 ($h_{\max}$) (%)	E_1 ($Q_{\max}^*$) (%)	E_1 ($h_{\max}$) (%)	E_1 ($Q_{\max}^*$) (%)	E_1 ($h_{\max}$) (%)	E_1 ($Q_{\max}^*$) (%)
1	10	39.97	14.07	14.15	15.69	11.60	17.02	10.02
2	19	19.98	13.97	5.09	17.49	7.57	19.82	7.88
3	37	9.99	10.54	2.94	11.66	4.26	13.49	3.94
4	72	5.07	7.23	2.95	9.22	2.29	10.68	2.40
5	141	2.57	5.54	2.02	6.14	1.25	7.37	1.02
6	281	1.29	3.41	0.74	3.26	0.62	3.51	0.54

Table 3. Sensitivity Analysis of the Predicted Arrival Time at the Outlet for Different Meshes and for Different Values of the Manning Coefficient

Mesh number	N	Spacing param. $\Delta x_m/y_{0m}$ (-)	$n_f = 0.05$ s/m$^{1/3}$ ε_w (%)	$n_f = 0.075$ s/m$^{1/3}$ ε_w (%)	$n_f = 0.10$ s/m$^{1/3}$ ε_w (%)
1	10	39.97	−162.17	−166.75	−171.09
2	19	19.98	−68.21	−73.70	−78.27
3	37	9.99	−37.50	−43.15	−47.66
4	72	5.07	−21.27	−24.92	−28.42
5	141	2.57	−9.89	−11.33	−12.94
6	281	1.29	−3.78	−4.40	−5.19

Table 4. Arrival Time at the Outlet and Main Statistics of the Maximum Water Depth and Discharge Calculated Based on Mesh 6 for Different Values of the Manning Coefficient

		h_{max} (m)				Q_{max} (10^3 m^3/s)			
n_f (s/m$^{1/3}$)	Arrival time (s)	Mean	25th percentile	50th percentile	75th percentile	Mean	25th percentile	50th percentile	75th percentile
0.05	152.10	16.27	12.87	15.81	18.42	21.20	21.17	21.26	21.42
0.075	202.41	18.60	15.58	18.31	20.99	20.23	19.84	20.88	21.13
0.10	247.41	20.39	17.30	20.24	23.09	19.47	18.67	20.12	20.91

The mesh size effect over the propagation time is shown in Table 3 for different values of n_f. Here the percentage deviation ε_w of the wetting front arrival time to the outlet with respect to the results obtained using Mesh 7 is reported. One can conclude that a coarse mesh, deteriorating the quality of the topographical representation, smooths the bed irregularity and, consequently, determines a quicker propagation of the wetting front of the dam-break wave.

The effect of the roughness parameter on the arrival time of the wetting front to the outlet section is presented in Table 4 adopting Mesh 6; the average celerity of this front increases by about 63% owing to a 50% reduction of the Manning coefficient (from 0.10 s/m$^{1/3}$ to 0.05 s/m$^{1/3}$). Table 4 also reports the main statistics concerning the spatial distribution of the maximum water level and discharge. An increase in the roughness raises the discharge peak reduction effect during the flood routing; actually, if n_f increases from 0.05 s/m$^{1/3}$ to 0.10 s/m$^{1/3}$, the mean value of Q_{max} decreases by about 8.4% and the whole discharge distribution translates toward smaller values. At the same time, the average maximum water depth increases by nearly 25%. However, since the valley presents very steep mountainsides along the examined reach, this variation in the maximum water depth does not significantly influence the extension of the flooded areas.

Finally, to evaluate the practical consequences of the uncertainty related to the dynamics of the failure, we have simulated the dam-break wave propagation (on Mesh 6, setting $n_f = 0.10$ s/m$^{1/3}$) hypothesizing both the instantaneous collapse (Scenario A) and an overall failure time of 1 min (Scenario B), as discussed in the "Boundary Conditions" section (Fig. 6). The profiles of the ratio of maximum discharges ($Q_{max}, B/Q_{max}, A$) and maximum water levels ($h_{max}, B/h_{max}, A$) computed according to these two scenarios are not much smaller than unity; the spatial distribution of the variable $Q_{max}, B/Q_{max}, A$ has mean value of 0.953 and standard deviation of 0.0104, whereas the mean value of $h_{max}, B/h_{max}, A$ is equal to 0.980 with standard deviation of 0.0068. Consequently, we conclude that in this case study the uncertainties on the collapse dynamics do not produce practical differences in terms of maximum values of water depth and discharge.

Results and Discussion

The numerical propagation of the Gleno dam-break wave along the whole valley was accomplished using a nonuniform mesh with 1,337 cross-sections with an interdistance similar to that of Mesh 6 adopted in the sensitivity analysis. The simulation was extended for a computational time of 2 h to completely describe the flood, as far as the valley outlet.

In consideration of the substantial morphological uniformity of the valley, a constant value for the roughness parameter in all the computational domain was assumed. The Manning coefficient was set at 0.09 s/m$^{1/3}$ by means of a calibration procedure based on the historical testimonies regarding the arrival time of the flooding at the village of Darfo (about 50 min after the dam break). An overall volume error in the order of 0.05% with respect to the volume initially stored in the Gleno reservoir was accepted.

Fig. 8 shows a synthesis of the numerical results. In particular, Fig. 8(a) represents some discharge hydrographs at the cross-sections shown in Fig. 4. The peak discharge decreases by almost 90%, from about 21,000 m^3/s at the dam site to about 2,000 m^3/s at Darfo. In the upper reach of the valley (along the first 3 km downstream of the dam, up to the village of Bueggio), the peak reduction effect is mild (7%) because the strong slope of the bottom (19% on average, with values locally even greater than 80%) determines a practically kinematic wave routing. The propagation presents similar character as far as the confluence between the Povo River and the Dezzo River. Considerable reductions of the peak discharge arise where the valley expands considerably, as at the site denominated "Rovina dei Cani e dei Ladri" (a broad depression located downstream of the village of Dezzo, upstream of Section 476 in Fig. 4) and at the wide plain upstream of the village of Gorzone in the lower part of the valley (upstream of Section 1,298 in Fig. 4).

Fig. 8(b) shows the water depth time series during the event at the same cross-sections: almost everywhere the maximum water stage exceeds 10 m, with peak values even greater than 30 m in the narrowest stretches of the valley. Water level sensibly increases in correspondence of strong valley contractions. Downstream of Section 476, the Dezzo river enters into a deep and narrow gorge. As a consequence, a temporary lake develops in about 6 min, flooding a 700 m stretch of the valley upstream and reaching a maximum

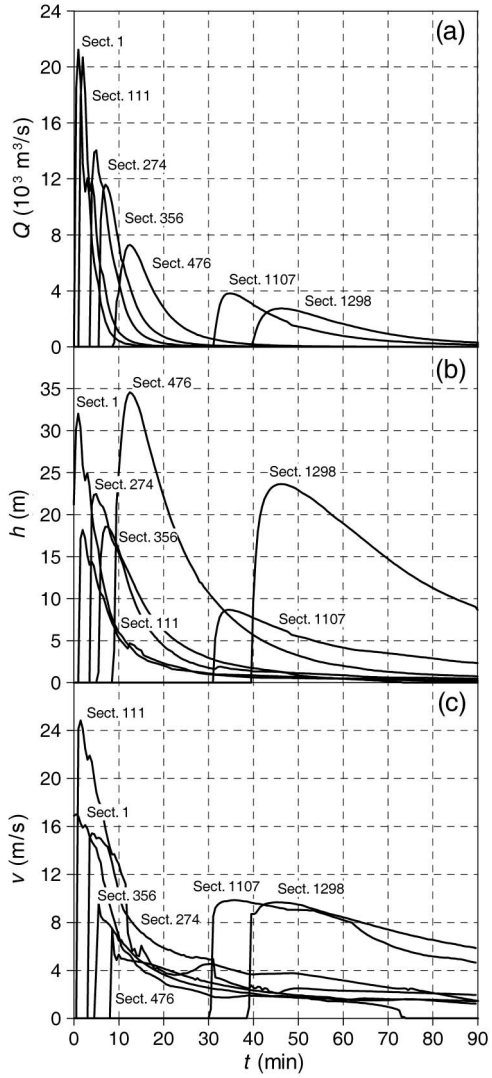

Fig. 8. (a) Discharge, (b) water level, and (c) average flow velocity time series computed at some selected cross sections

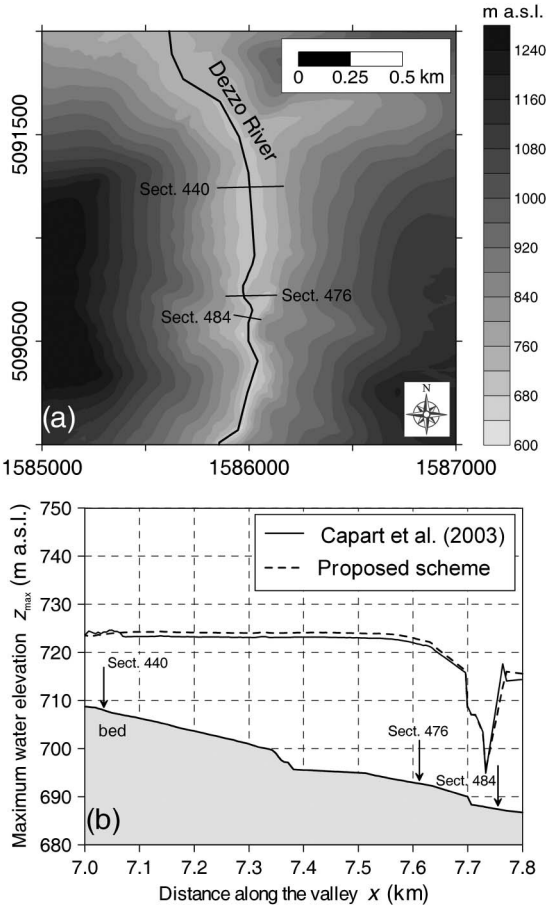

Fig. 9. (a) Contour map of the bathymetry of the Rovina dei Cani e dei Ladri site [Italian Gauss-Boaga reference system (m)]; (b) comparison between maximum water elevation envelopes calculated by means of the two considered numerical schemes ($\Delta x = 5$ m)

water level of nearly 30 m. The historical documents confirm the formation of this lake during the inundation; in accordance with the testimonies, in consequence of this water accumulation, the upstream village of Dezzo ran the risk of being flooded by backwater. A similar phenomenon took place near the village of Gorzone, where the backwater effect threatened the village of Angolo and destroyed a reach of the provincial road. The presented numerical model, despite the nonconservative feature, is capable of reproducing these salient characteristics with a very satisfactory accordance with the results derived from the application of the original scheme by Capart et al. (2003), as shown by Fig. 9, which compares the envelopes of maximum water surface elevation along the Rovina dei Cani e dei Ladri enlargement obtained with the two numerical schemes using a very fine mesh with a cross-section spacing of about 5 m.

The maximum averaged velocity exceeds 5 m/s everywhere and presents values even greater than 20 m/s in the very steep upper reach of the valley and in the narrowest stretches [Fig. 8(c)]. Table 5 provides quantitative information concerning the timing of the dam-break wave deduced from the numerical simulation; the passage of the wave in some significant sites along the valley (shown in Fig. 4) is considered. The flood reaches the first villages (e.g., Bueggio) in a few minutes and exhausts itself (e.g., when the discharge reduces to 1/100 of the peak value) very rapidly, in confirmation of the impulsive and destructive character of the event. The closeness between the arrival time of the wetting

Table 5. Numerical Results Concerning the Timing of the Gleno Dam-Break Routing

Section number	Distance along the valley (km)	Wetting front arrival time (min)	Peak			Wave Duration (min)
			Timing (min)	Discharge (m^3/s)	Water depth (m)	
111 (Bueggio)	1.731	1.0	2.0	20824	18.2	14
356 (Dezzo)	5.694	5.5	7.0	11610	18.6	25
1107 (Mazzunno)	17.850	27.5	34.5	3825	8.7	93
1326 (Darfo)	21.373	40.5	47.0	2741	14.1	—

Table 6. Comparison between Estimated and Calculated Maximum Water Depths at Some Locations

Water marks	Section number	Distance along the valley (km)	Maximum water depth estimated (m)	Maximum water depth calculated (m)	Error (%)
A (Dezzo Bridge)	357	5.709	16–17	18.5	(+8.8)–(+15.6)
B (Fusinoni Tunnel)	465	7.440	31–34	32.9	(−3.2)–(+6.1)
C (Angolo Bridge)	1,196	19.292	22	19.7	−10
D (Gorzone, Federici's Monument)	1,296	20.890	30–32	26	(−13.3)–(−18.7)

front and the peak discharge (or peak water depth without appreciable distinction), especially in the selected sections located in the upper stretch of the valley, indicates that the water profile presents a very steep front, which is typical of waves propagating in very sloping streams.

Since the timing of the event is not documented in a reliable way along the valley, the verification of the numerical model performance in peak timing prediction is not possible. However, when the flood dynamics are very fast, as in this case study and generally in the occurrence of dam break, the flood timing is not a parameter as significant for the hydraulic hazard assessment as the envelope of the maximum water stages.

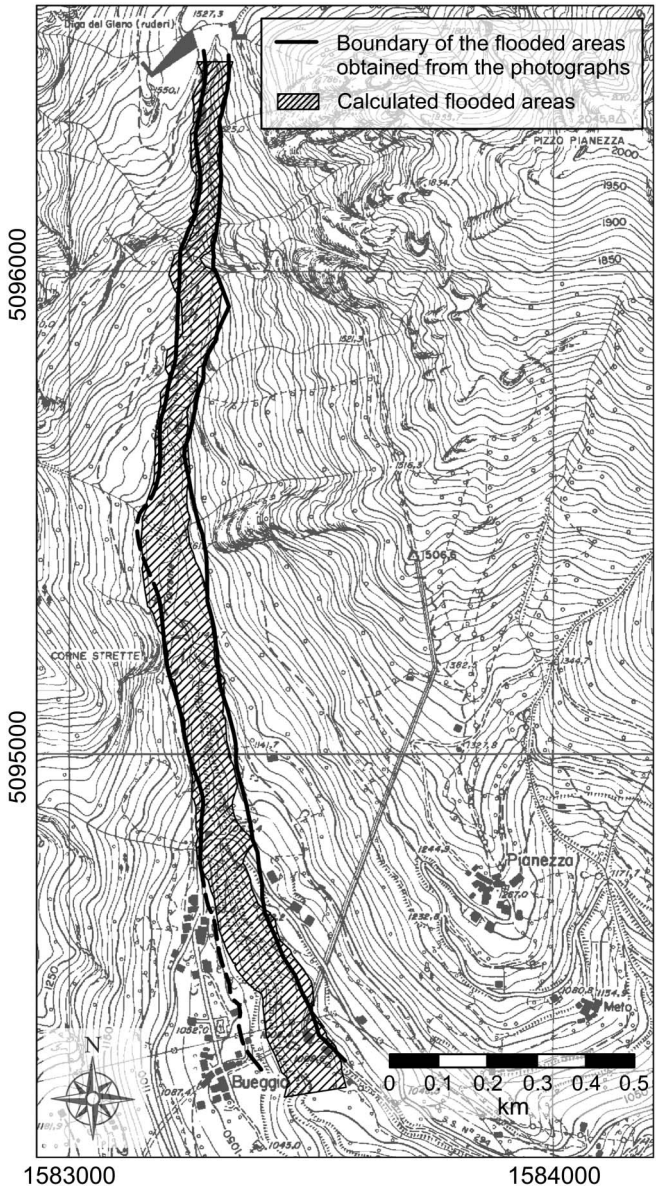

Fig. 10. Comparison between imaging estimation and numerical prediction of the inundated area extent for the reach just downstream of the dam [Italian Gauss-Boaga reference system (m)]

The computation of the envelope of highest water depths allows reconstruction of the boundaries of the inundated area that can be compared with those obtained from the historical photographs. Fig. 10 shows this comparison with reference to a stretch just downstream of the dam. Where the historical documents do not allow certain definition of the inundated region, an interpolated contour line (dashed in Fig. 10) is drawn. The numerical simulation confirms the submersion of the Povo, Valbona, and Mazzunno powerhouses and allows an estimate of about 1.60 km^2 for the inundated areas.

Finally, Table 6 compares the computed maximum water depth with the corresponding estimation derived from historical information for the water marks pointed out in Fig. 4. Although the Water Marks C and D are located just upstream of strong valley contractions where certainly blockage due to floating debris increased the backwater effect, on the whole, we observe a more than satisfactory agreement between numerical results and field data.

Conclusions

This paper revisits the Gleno accident, the most important Italian dam-break case, which occurred in a small alpine valley in 1923, and provided its first hydraulic reconstruction. Based on testimonies from the eyewitness, the dynamics and timing of the failure were reasonably reconstructed, and the extent of the water flooding along the valley has been identified by applying a georeferentiation procedure to several historical pictures taken shortly after the accident. This has allowed an estimate of the maximum flood extent envelope for more than 5 km along the valley. In addition, based on the historical documents, the maximum water depth at some locations have been obtained. The bed bathymetry of the valley, mostly carved in rocks, has been reconstructed based on a DEM that has been locally reshaped to take into account the most relevant local erosion processes that have been triggered by the wave passage. This test case is made available to the scientific community at the ASCE Library (http://www.ascelibrary.org) and at the website http://www.ing.unibs.it/~idraulica/gleno_testcase.htm.

As a second contribution, the accident has been modeled by using the SWEs. The detailed description of the reservoir bathymetry along with the information regarding the breach formation have allowed a 2D shallow-water simulation of the reservoir emptying, providing a peak discharge of about 21,000 m^3/s at the dam site. Then, the 1D shallow water modeling of the dam-break wave propagation, accomplished by using a recently proposed algorithm for natural bathymetries, indicates a strong peak reduction effect; the value of the peak discharge halves only 5 km downstream of the dam location and at the end of the valley the maximum discharge (of about 2,000 m^3/s) is four times greater than the corresponding millenary flood. The numerical extent of the flooded areas and the calculated maximum water levels agree fairly well with those

reconstructed based on historical documents. The adopted numerical scheme proves to be an effective and robust tool, but requires a very fine mesh in the presence of steep slopes. The simple adaptation proposed here partly overcomes this difficulty by maintaining the positive features of the original scheme and improving its effectiveness in mountain environments.

This modeling effort has also offered the opportunity to test the importance of some choices that have to be made when modeling similar events. These mainly regard the level of detail needed for the hydrograph at the dam section and the size of the computational grid. With reference to the former, the analysis of two different time failure scenarios leads to the conclusion that limited variations in the dynamics of the collapse have a negligible practical influence on the spatial envelope of maximum values of water depth and discharge. The sensitivity analysis accomplished concerning mesh size has shown that an average spacing of about 16 m provides a good numerical convergence and is suitable for an accurate description of the event.

Finally, we have come to the conclusion that the 1D shallow water mathematical model, even if based on restrictive hypotheses, is capable of reproducing the main macroscale hydraulic characteristics of the event. Consequently, where the 1D schematization is realistic, as in our case, this model is suitable to predict a dam-break flow even over the irregular and very steep topographies typical of mountain streams and can be effectively employed to estimate the most significant parameters of interest for hydraulic hazard assessment.

Acknowledgments

We greatly appreciated the helpful cooperation of Eng. Simone Bonetti and all the people and agencies that allowed the collection of the documentary information. We sincerely thank the photographer's studio Foto Giorgio (http://www.scalve.it/) that provided many of the historical pictures used in this work. Finally, we would like to thank the reviewers and the editor, whose valuable suggestions contributed to improve the quality of this paper.

Supplemental Data

The following supplementary data files are available online at the ASCE Library (www.ascelibrary.org):

File S1: Ancillary figures

File S2: Details concerning the upstream boundary condition used in the numerical simulations

File S3: DEM of the valley

File S4: Selected historical documents concerning the event

File S5: Outline of the flooded area estimated from historical documents

File S6: DEM of the Gleno Reservoir

File S7: Frames of the 2D numerical reconstruction of the Gleno Reservoir emptying

File S8: Pictures showing the Gleno Dam remains as presently visible

File S9: Topographical maps of the valley

File S10: Selection of pictures concerning the Gleno disaster

File S11: Main results of the numerical simulations

File S12: Topographic description of the channel thalweg

File S13: Pictures useful for estimating the roughness of the channel

File S14: Geometric elements of the cross sections

File S15: List of major documentary sources

File S16: Examples of superimposition of historical pictures and 3D virtual images

File S17: Water marks

References

Alcrudo, F., and Mulet, J. (2007). "Description of the Tous dam-break case study (Spain)." *J. Hydraul. Res.*, 45 (Extra Issue), 45–57.

Associazione Nazionale Imprese Produttrici e Distributrici di Energia Elettrica (ANIDEL). (1961). *Le dighe di ritenuta degli impianti idroelettrici italiani*, Vol. 1, ANIDEL, Rome, Italy (in Italian).

Aureli, F., Maranzoni, A., Mignosa, P., and Ziveri, C. (2008a). "Dam-break flows: Acquisition of experimental data through an imaging technique and 2D numerical modeling." *J. Hydraul. Eng.*, 134(8), 1089–1101.

Aureli, F., Maranzoni, A., Mignosa, P., and Ziveri, C. (2008b). "2D numerical modelling for hydraulic hazard assessment: A dam-break case study." *Proc., Int. Conf. on Fluvial Hydraulics, River Flow 2008*, Kubaba Congress Dept. and Travel Services, Ankara, Turkey, 729–736.

Barnes, H. H., Jr. (1967). "Roughness characteristics of natural channels." *Paper 1849*, U.S. Geological Survey, Water Supply, Denver.

Begnudelli, L., and Sanders, B. F. (2007). "Simulation of the St. Francis dam-break flood." *J. Eng. Mech.*, 133(11), 1200–1212.

Braschi, G., and Gallati, M. (1992). "A conservative flux prediction algorithm for the explicit computation of transcritical flow in natural streams." *Proc., Hydrosoft '92*, Computational Mechanics Publications, Southampton, UK, 381–394.

Capart, H., Bogaerts, C., Kevers-Leclercq, J., and Zech, Y. (1999). "Robust numerical treatment of flow transitions at drainage pipe boundaries." *Water Sci. Technol.*, 39(9), 113–120.

Capart, H., Eldho, T. I., Huang, S. Y., Young, D. L., and Zech, Y. (2003). "Treatment of natural geometry in finite volume river flow computations." *J. Hydraul. Eng.*, 129(5), 385–393.

Capart, H., Eldho, T. I., Huang, S. Y., Young, D. L., and Zech, Y. (2004). "Closure to 'Treatment of natural geometry in finite volume river flow computations' by H. Capart, T. I. Eldho, S. Y. Huang, D. L Young, and Y. Zech." *J. Hydraul. Eng.*, 130(10), 1048–1049.

Capart, H., and Young, D. L. (1998). "Formation of a jump by the dam-break wave over a granular bed." *J. Fluid Mech.*, 372, 165–187.

Capart, H., et al. (2007). "The 1996 Lake Ha! Ha! breakout flood, Québec: Test data for geomorphic flood routing methods." *J. Hydraul. Res.*, 45 (Extra Issue), 97–109.

Chen, J., Steffler, P. M., and Hicks, F. E. (2007). "Conservative formulation for natural open channels and finite-element implementation." *J. Hydraul. Eng.*, 133(9), 1064–1073.

Concerted Action on Dambreak Modelling (CADAM). (1999). Papers 1–12. *Proc., 4th CADAM meeting* (online), Univ. of Zaragoza, Spain, ⟨http://www.hrwallingford.co.uk/projects/CADAM/CADAM/index.html⟩.

Cunge, J. A., Holly, F. M., Jr., and Verwey, A. (1980). *Practical aspects of computational river hydraulics*, Pitman Publishing, London.

De Marchi, G. (1945). "Sull'onda di piena che seguirebbe al crollo della diga di Cancano." *L'Energia Elettrica*, 22, 319–340 (in Italian).

De Martini, A. (1924). "Details of the failure of an Italian multiple-arch dam." *Eng. News-Rec.*, 92(5), 182–184.

Donnelly, C. R., and Morgenroth, M. (2005). "Risky business for dams." *Int. Water Power Dam Constr.*, 57(5), 16–23.

Douglas, K. J., Spannagle, M., and Fell, R. (1998). "Analysis of concrete and masonry dam incidents." *Rep. R-373*, New South Wales University, Sydney, Australia.

Ganassini, G., and Danusso, A. (1924). "Relazione peritale sopra le cause che hanno determinato la rovina della diga del Pian del Gleno in Val di Scalve, crollata la mattina del 1 dicembre." *Annali dei LL. PP.*, 5, 405–435 (in Italian).

Garcia, M. H. (2007). "Foreword." *J. Hydraul. Res.*, 45 (Extra Issue), 3.

Garcia-Navarro, P., Fras, A., and Villanueva, I. (1999). "Dam-break flow simulation: Some results for one-dimensional models of real cases." *J. Hydrol. (Amsterdam)*, 216(3-4), 227–247.

Goutal, N. (1999). "The Malpasset dam failure. An overview and test case definition." *Proc., 4th CADAM meeting* (online), Univ. of Zaragoza, Spain, ⟨http://www.hrwallingford.co.uk/projects/CADAM/CADAM/Zaragoza/Contents.html⟩.

Hardy, R. J., Bates, P. D., and Anderson, M. G. (1999). "The importance of spatial resolution in hydraulic models for floodplain environments." *J. Hydrol. (Amsterdam)*, 216(1-2), 124–136.

Hervouet, J. M., and Petitjean, A. (1999). "Malpasset dam-break revisited with two-dimensional computation." *J. Hydraul. Res.*, 37(6), 777–788.

James, L. B. (1988). "The failure of Malpasset dam." *Advanced dam engineering for design, construction, and rehabilitation*, Van Nostrand Reinhold, New York, 17–27.

Jarrett, R. D. (1984). "Hydraulics of high gradient streams." *J. Hydraul. Eng.*, 110(11), 1519–1539.

Jarrett, R. D., and Costa, J. E. (1986). "Hydrology, geomorphology, and dam-break modelling of the July 15, 1982 Lawn Lake Dam and Cascade Lake Dam failures, Larimer County, Colorado." *Professional Paper 1369*, U. S. Geological Survey, Denver.

Johnson, F. A., and Illes, P. (1976). "A classification of dam failures." *Int. Water Power Dam Constr.*, 28(12), 43–45.

LeVeque, R. J. (2002). *Finite volume methods for hyperbolic problems*, Cambridge University Press, Cambridge, UK.

Maugliani, V. (2004). "Elementi salienti del disastro della diga del Gleno ed evoluzione della normativa italiana sulle dighe." *L'Acqua*, 2, 31–52 (in Italian).

Mohapatra, P. K., and Chaudhry, M. H. (2004). "Numerical solution of Boussinesq equations to simulate dam-break flows." *J. Hydraul. Eng.*, 130(2), 156–159.

Natale, L., Petaccia, G., and Savi, F. (2008). "Simulation of Sella Zerbino catastrophic dam-break." *Proc., Int. Conf. on Fluvial Hydraulics, River Flow 2008*, Kubaba Congress Dept. and Travel Services, Ankara, Turkey, 601–607.

Pedersoli, G. S. (1973). *Il Gleno. Storia ed album fotografico*, Edizioni Toroselle, Bergamo, Italy (in Italian).

Pilotti, M., Maranzoni, A., and Tomirotti, M. (2006). "An efficient tool for hydraulic hazard analysis in alpine valleys." *Proc., 7th Int. Conf. on Hydroinformatics*, Research Publishing Services, Chennai, India, 2276–2283.

Pilotti, M., Tomirotti, M., Valerio, G., and Bacchi, B. (2010). "A simplified method for the characterization of the hydrograph following a sudden partial dam break." *J. Hydraul. Eng.*, 136(10), 693–704.

Samuels, P. G. (1990). "Cross-section location in 1-D models." *Proc., Int. Conf. on River Flood Hydraulics*, Wiley, Chichester, UK, 339–350.

Saxena, K. R., and Sharma, V. M. (2004). *Dams: Incidents and accidents*, Taylor & Francis, New York.

Singh, V. P. (1996). *Dam-break Modelling Technology*, Kluwer Academic, Dordrecht, The Netherlands.

Soares Frazão, S., Morris, M. W., and Zech, Y., eds. (2000). "Concerted action on dambreak modelling: Objectives, project report, test cases, meeting proceedings." (CD-ROM), Civil Engineering Dept., Hydraulics Div., Université Catholique de Louvain, Louvain-la-Neuve, Belgium.

Soares Frazão, S., and Zech, Y. (2007). "Experimental study of dam-break flow against an isolated obstacle." *J. Hydraul. Res.*, 45 (Extra Issue), 27–36.

Soares Frazão, S., Zech, Y., and Morris, M., eds. (2003). "IMPACT, Investigation of extreme flood processes and uncertainty." *3rd Project Workshop Proc.* (CD-ROM), Civil Engineering Dept., Hydraulics Div., Université Catholique de Louvain, Louvain-la-Neuve, Belgium.

Spinewine, B., and Zech, Y. (2007). "Small-scale laboratory dam-break waves on movable bed." *J. Hydraul. Res.*, 45 (Extra Issue), 73–86.

Stucky, A. (1924). "La rupture du barrage du Gleno." *Bull. Tech. Suisse Romande*, 50(6–7), 65–71, 79–82 (in French).

Toro, E. F. (2001). *Shock-capturing methods for free-surface shallow flows*, Wiley, Chichester, UK.

Valiani, A., Caleffi, V., and Zanni, A. (2002). "Case study: Malpasset dam-break simulation using a two-dimensional finite volume method." *J. Hydraul. Eng.*, 128(5), 460–472.